Photochemistry and Photobiology, 2008, 84: 1061–1072

Examination of Chlorin–Bacteriochlorin Energy-transfer Dyads as Prototypes for Near-infrared Molecular Imaging Probes†

Hooi Ling Kee[1], Ralph Nothdurft[2], Chinnasamy Muthiah[3], James R. Diers[4], Dazhong Fan[3], Marcin Ptaszek[3], David F. Bocian[4], Jonathan S. Lindsey[3], Joseph P. Culver[2] and Dewey Holten*[1]

[1]Department of Chemistry, Washington University, St. Louis, MO
[2]Department of Radiology, Washington University, St. Louis, MO
[3]Department of Chemistry, North Carolina State University, Raleigh, NC
[4]Department of Chemistry, University of California Riverside, Riverside, CA

Received 18 April 2008, accepted 22 May 2008, DOI: 10.1111/j.1751-1097.2008.00409.x

ABSTRACT

New classes of synthetic chlorin and bacteriochlorin macrocycles are characterized by narrow spectral widths, tunable absorption and fluorescence features across the red and near-infrared (NIR) regions, tunable excited-state lifetimes (< 1 to > 10 ns) and chemical stability. Such properties make dyad constructs based on synthetic chlorin and bacteriochlorin units intriguing candidates for the development of NIR molecular imaging probes. In this study, two such dyads (FbC-FbB and ZnC-FbB) were investigated. The dyads contain either a free base (Fb) or zinc (Zn) chlorin (C) as the energy donor and a free base bacteriochlorin (B) as the energy acceptor. In both constructs, energy transfer from the chlorin to bacteriochlorin occurs with a rate constant of $\sim(5\ \text{ps})^{-1}$ and a yield of > 99%. Thus, each dyad effectively behaves as a single chromophore with an exceptionally large Stokes shift (85 nm for FbC-FbB and 110 nm for ZnC-FbB) between the red-region absorption of the chlorin and the NIR fluorescence of the bacteriochlorin ($\lambda_f = 760$ nm, $\Phi_f = 0.19$, $\tau \sim 5.5$ ns in toluene). The long-wavelength transitions (absorption, emission) of each constituent of each dyad exhibit narrow (≤20 nm) spectral widths. The narrow spectral widths enabled excellent selectivity in excitation and detection of one chlorin–bacteriochlorin energy-transfer dyad in the presence of the other upon diffuse optical tomography of solution-phase phantoms.

INTRODUCTION

Optical imaging offers a new approach for *in vivo* medical diagnostics as well as treatment of diseased tissues (1–16). The success of optical imaging depends in large part on the availability of molecular probes that meet a demanding set of photophysical criteria, including (1) intense absorption and efficient emission in the red or near-infrared (NIR) spectral region, (2) sharp absorption and emission bands, (3) large absorption-fluorescence spacing (Stokes shift), (4) long excited-state lifetime and (5) photostability. The NIR spectral region (700–900 nm) is of interest because absorption by endogenous species (*e.g.* hemoglobin, proteins) is low, penetration of light several centimeters enables deep tissue imaging, and background emission and light scattering are reduced compared to visible wavelengths (13,15). A large absorption-fluorescence spacing (Stokes shift) facilitates the ability to prevent scattered excitation light from reaching the fluorescence detection system, which compromises image quality. Sharp absorption and emission bands facilitate selective excitation/detection and thereby enable simultaneous use of multiple probes. Other desirable features include ease of synthesis, high stability, tailorable solubility, provisions for bioconjugation, absence of toxicity, biological targetability and systemic clearance. No optical probes satisfactorily meet all of these photophysical, chemical and physiological criteria.

The ongoing development of optical probes is an arduous undertaking that encompasses molecular design, chemical synthesis, photophysical characterization and evaluation *in vitro* and *in vivo*. The results of the biological studies typically are coupled with photophysical insights and advances in synthetic chemistry in a new cycle of development to achieve enhanced performance. The path is often tortuous and can span decades. The cyanine dyes, for example, were first discovered in the 19th century (17), extensively developed in the early 20th century for use as sensitizers in photography (18,19), and derivatized beginning in the late 1980s for biological applications as fluorophores (20–24). A chief attraction that prompted focus on the cyanine dyes for biological applications was their wavelength tunability upon structural modification. Intense development of the chemistry over the ensuing two decades has yielded the family of water-soluble bioconjugatable cyanine probes that are in widespread use in the biomedical sciences (25). The most prominent examples used for optical imaging include indocyanine green and its cypate derivatives (9,26), the water-soluble cyanines (Cy5, Cy5.5, Cy7, *etc.*) developed by Waggoner and coworkers (20–24), and the analogous series of Alexa Fluor (AF) probes (27,28). The development and evaluation of novel cyanine-based optical probes remains an ongoing and fertile area of research (29–32).

Tetrapyrrole macrocycles also afford wavelength tunability upon progressive reduction of the macrocycle. Porphyrins absorb only weakly in the red region of the spectrum (600–700 nm) and not at all in the NIR region, whereas chlorins (dihydroporphyrins) absorb strongly in the red region, and

†This invited paper is part of the Series: Applications of Imaging to Biological and Photobiological Systems.

*Corresponding author email: holten@wustl.edu (Dewey Holten)

bacteriochlorins (tetrahydroporphyrins) absorb even more strongly in the NIR region (33). To date, the chlorins and bacteriochlorins employed for optical imaging have mainly been derived from chlorophyll *a* or bacteriochlorophyll *a* (26,34). The natural chlorins and bacteriochlorins have somewhat limited synthetic malleability (35), tend to aggregate, and in some cases are prone to oxidation to the porphyrin or chlorin, respectively (36,37). The development of *de novo* synthetic routes has provided access to stable chlorins and bacteriochlorins (38–45). The synthetic chlorins and bacteriochlorins shown in Chart 1 are stable toward adventitious dehydrogenation due to the presence of a geminal dimethyl group in each reduced pyrrole ring. The methodology is compatible with the incorporation of a wide range of substituents to enhance solubility in organic or aqueous media (thereby inhibiting aggregation) and to provide synthetic handles for bioconjugation and biotargeting. Indeed, water-soluble versions of the chlorins (46) and bacteriochlorins (47) were recently prepared. Furthermore, the *de novo* synthetic methods allow access to multiply substituted chlorins or bacteriochlorins that display wide tunability of the redox and photophysical properties, including absorption and fluorescence wavelengths (600 nm to at least 800 nm) and fluorescence lifetimes (1–13 ns) for free base complexes and zinc chelates (41,42,44). The red and NIR features are spectrally narrow (full-width-at-half-maximum [FWHM] ≤20 nm and often < 15 nm). These and other photophysical characteristics make these constructs very appealing for consideration in optical imaging applications.

The challenge of obtaining strong absorption and fluorescence in the NIR and large wavelength spacing between these features has prompted the development of energy-transfer dyads (tandem probes). In such tandem probes, the donor is selected for absorption properties and the acceptor is chosen for emission properties. In the ideal construct, energy transfer from donor to acceptor chromophores is so efficient (and fast) that effectively the dyad behaves like a single chromophore, but with a large spacing between the red or NIR absorption and emission bands. Prominent examples include cyanine dyes conjugated to phycobilisome subunits (48–50), which have been used in flow cytometry, but are quite large for optical imaging applications.

Numerous energy-transfer dyads have been synthesized that incorporate members of the tetrapyrrole family (porphyrins, chlorins, oxochlorins, phthalocyanines) and other chromophores (51–53). Mechanistic studies have elucidated the design principles (linker type, attachment sites, orbital characteristics) that produce ultrafast and essentially quantitative excited-state energy transfer in such dyads (52). This knowledge has been used in the design of the two compact chlorin–bacteriochlorin (C–B) dyads (and benchmark monomers) shown in Chart 2. The dyads (**FbC-FbB** and **ZnC-FbB**) incorporate either a free base (Fb) or zinc (Zn) chlorin (C) as the energy donor and a free base bacteriochlorin (B) as the energy acceptor. The photophysical characteristics of **FbC-FbB** and reference monomers have been reported (53). In brief, energy transfer from the excited chlorin to bacteriochlorin in **FbC-FbB** occurs with a rate constant of $(4.8\ \text{ps})^{-1}$ and a yield of >99% in toluene. Excitation of the chlorin in its red-region absorption maximum (675 nm) results in fluorescence from the bacteriochlorin (760 nm) with essentially the same fluorescence yield (0.19) and singlet excited-state lifetime (5.4 ns) found in the bacteriochlorin building block. Thus, the **FbC-FbB** behaves as though it were a monomeric probe with an 85 nm Stokes shift between narrow (FWHM ≤20 nm) absorption and fluorescence bands.

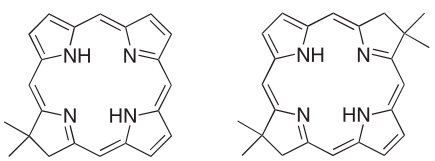

chlorin bacteriochlorin

Chart 1.

In this study, we present the synthesis and characterization of a companion dyad **ZnC-FbB** that exhibits an even larger effective Stokes shift (110 nm). The objectives of this study are to (1) assess the spectral properties of such dyads for optical imaging, and if suitable, (2) guide the design of analogues appropriate for optical imaging. Because both **FbC-FbB** and **ZnC-FbB** are soluble in organic solvents (not aqueous media) and lack the structural motifs required for bioconjugation and biotargeting, solution-phase phantoms were employed. The phantoms were examined with a diffuse optical tomography imager (54). Studies with phantoms (55) do not require structural provisions for water solubility and bioconjugatability, can be made across different classes of fluorophores without the data being confounded by differences in biolocalization of the different fluorophores, and provide a valuable means for interim evaluation of prototypical chromophores. Regardless, it is known that tetrapyrrole chromophores exhibit almost identical spectral and photophysical attributes in organic and aqueous media if homogeneously dispersed (46). The **FbC-FbB** and **ZnC-FbB** dyads are compared with two commercially available cyanine dyes that have absorption and fluorescence maxima in the same spectral regions. A key focus of the comparisons is the relative selectivity of the two classes of probes in both absorption and fluorescence. Such selectivity is important in defining the attributes for multi-probe (multicolor) applications, including site discrimination, contrast and the number of detection channels that can be accommodated in a specific spectral window.

MATERIALS AND METHODS

Dyads and monomers. Dyad **FbC-FbB** has been described previously (53), as have two reference monomers (53): 3,13-bis(2-phenylethynyl)-17,18-dihydro-18,18-dimethyl-10-(4-ethynylphenyl)porphyrin (**FbC1**) and 5-methoxy-15-(2-phenylethynyl)-8,8,18,18-tetramethyl-2,12-di-*p*-tolylbacteriochlorin (**FbB1**).

*Metalation. 15-[2-[4-[Zn(II)-3,13-bis(2-phenylethynyl)-17,18-dihydro-18,18-dimethylporphin-10-yl]phenyl]ethynyl]-5-methoxy-8,8,18,18-tetramethyl-2,12-di-p-tolylbacteriochlorin (**ZnC-FbB**).* A solution of **FbC-FbB** (4.00 mg, 0.00327 mmol) in $CHCl_3$/methanol (2.0 mL, [4:1]) was treated with $Zn(OAc)_2{\cdot}2H_2O$ (21.6 mg, 0.0984 mmol). The reaction mixture was stirred at room temperature for 4 h. CH_2Cl_2 was added, and the reaction mixture was washed with water and brine. The organic layer was separated, dried (Na_2SO_4) and concentrated. The resulting crude solid was dissolved in CH_2Cl_2. The solution was filtered through a pad of silica (CH_2Cl_2). The filtrate was concentrated to afford a green solid (3.9 mg, 93%): ^{1}H NMR (400 MHz, $CDCl_3$) δ –1.51 (brs, 1H), –1.19 (brs, 1H), 1.91 (s, 6H), 2.00 (s, 6H), 2.02 (s, 3H), 2.06 (s, 3H), 2.62 (s, 6H), 4.16–4.35 (m, 5H), 4.57–4.60 (m, 2H), 4.78

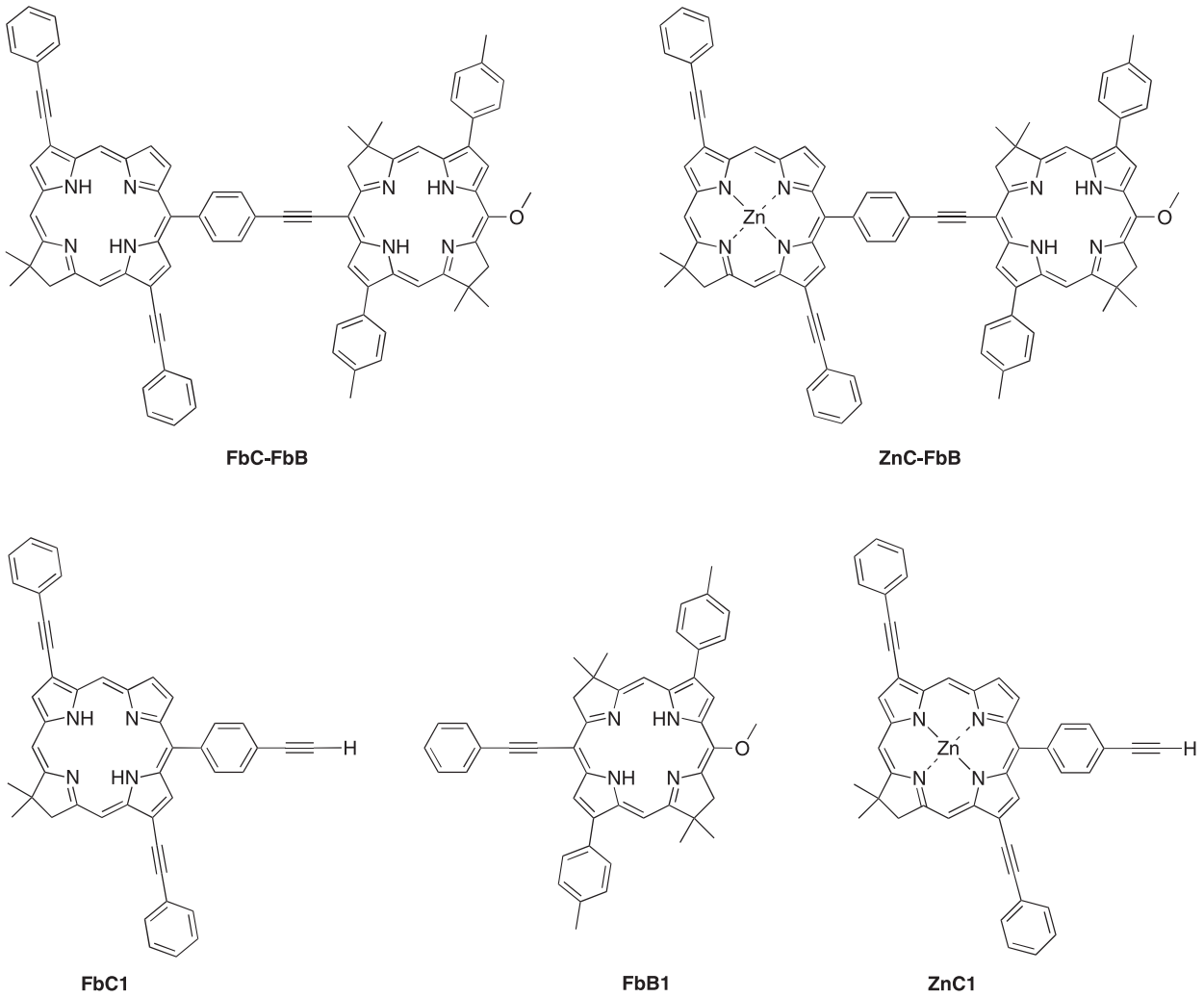

Chart 2.

(s, 2H), 7.18–7.62 (m, 10H), 7.84–8.20 (m, 12H), 8.42 (s, 1H), 8.55–8.60 (m, 1H), 8.73 (s, 1H), 8.82 (brs, 2H), 8.88 (d, J = 4.4 Hz, 1H), 8.92–8.96 (m, 1H), 9.04–9.08 (m, 1H), 9.31 (s, 1H), 9.67 (s, 1H), 9.91 (s, 1H); LD-MS obsd 1283.3; FAB-MS obsd 1280.4812, calcd 1280.4808 ($C_{85}H_{68}N_8OZn$); λ_{abs} (CH_2Cl_2) 386, 426, 556, 650, 755 nm.

*Zn(II)-3,13-Bis(2-phenylethynyl)-17,18-dihydro-18,18-dimethyl-10-(4-ethynylphenyl)porphyrin (**ZnC1**)*. A solution of **FbC1** (2.40 mg, 0.00374 mmol) in $CHCl_3$/methanol (2.0 mL, [4:1]) was treated with $Zn(OAc)_2{\cdot}2H_2O$ (24.6 mg, 1.12 mmol). The reaction mixture was stirred at room temperature. After 4 h, the reaction mixture was concentrated. The resulting crude solid was filtered through a pad of silica (hexanes then hexanes/CH_2Cl_2 [1:2]). The filtrate was concentrated to afford a green solid (2.30 mg, 91%): ^{1}H NMR (400 MHz, $CDCl_3$) δ 2.04 (s, 6H), 3.30 (s, 1H), 4.56 (s, 2H), 7.44–7.58 (m, 6H), 7.82–7.90 (m, 4H), 7.93 (d, J = 7.6 Hz, 2H), 8.04 (d, J = 7.6 Hz, 2H), 8.47 (d, J = 4.4 Hz, 1H), 8.54 (s, 1H), 8.77 (s, 1H), 8.86 (s, 1H), 8.87 (d, J = 4.4 Hz, 1H), 9.04 (s, 1H), 9.80 (s, 1H); LD-MS obsd 702.2; FAB-MS obsd 702.1758, calcd 702.1762 ($C_{46}H_{30}N_4Zn$); λ_{abs} (toluene) 427, 652 nm; Φ_f (toluene) = 0.33; singlet excited-state lifetime (toluene) = 3.8 $\pm$ 0.2 ns.

Photophysical characterization. Photophysical measurements were performed using the same instrumentation and sample conditions described previously for **FbC-FbB** and **FbC1** (53). The fluorescence quantum yield of each AF dye was determined relative to chlorophyll *a* in benzene (Φ_f = 0.325 [56]) and free base tetraphenylporphyrin in toluene (Φ_f = 0.09 [57]), and were corrected for solvent refractive index, and the results averaged.

Optical imaging. Imaging studies were performed on phantoms of the two C–B dyads (**FbC-FbB** and **ZnC-FbB**) in toluene and two AF dyes (**AF647** and **AF680**) in aqueous PBS buffer (10 mM Na_3PO_4, 137 mM NaCl, 2.7 mM KCl, pH 7.4) adjusted to the same concentration (1 μM using the molar absorption coefficients given in Table 1). The studies utilized a fast scanning fluorescence diffuse optical tomography instrument designed for imaging the kinetics of probe distributions throughout the whole body of small animals (54). The instrument simultaneously provides optimal resolution, sensitivity, full body field-of-view and short scan times. The system is configured in a plane parallel geometry in which a source laser is scanned using a galvanometer mirror pair ($\tau_{switch} \sim 1$ ms) over flexible source patterns, and detects excitation and emission light using a high frame rate, low noise, 5 MHz electron-multiplied charge-coupled detector camera.

Pairwise comparisons were made by placing samples (in 3 mm ID tubes) of either the two C–B dyads or the two AF dyes in an optical imaging tank containing optical index matching fluid (54) at positions 15 or 35 mm along the 50 mm horizontal (X) direction, as is illustrated schematically in Fig. 1. The samples were centered in the imaging tank in the Z direction, which is the direction of propagation of the excitation laser beam. The laser was scanned along the X direction from 0 to 50 mm, displaced by 1 mm in the Y (vertical) direction, scanned again in the X direction and so on. Image reconstructions were performed based on the detected fluorescence (54). Here, 2D images for a top (X–Z) view are presented, as is illustrated in Fig. 1.

Table 1. Photophysical properties of chlorin–bacteriochlorin dyads and Alexa Fluor dyes.

Compound	Solvent	λ_{abs} (nm)	ε* (M^{-1} cm^{-1})	λ_{flu} (nm)	FWHM†	Φ_f	τ (ns)
FbC-FbB	Toluene	675‡	80 000	760	18	0.19	5.4
ZnC-FbB	Toluene	650‡	60 000	760	21	0.19	5.3
AF647	1× PBS	649	239 000	669	41	0.34	1.2
AF680	1× PBS	676	184 000	702	57	0.36	1.4

AF = Alexa Fluor; FWHM = full-width-at-half-maximum. *The molar absorption coefficients of the AF dyes were taken from the Invitrogen website (http://www.probes.invitrogen.com; accessed on 14 April 2008). The values for the chlorin component of the dyad were estimated based on the values determined in Muthiah *et al.* (53) for related compounds. †Average FWHM of the spectral features (not fully encompassing the broad shoulders for the AF dyes; see Figs. 4 and 5). ‡For the chlorin component of the dyad.

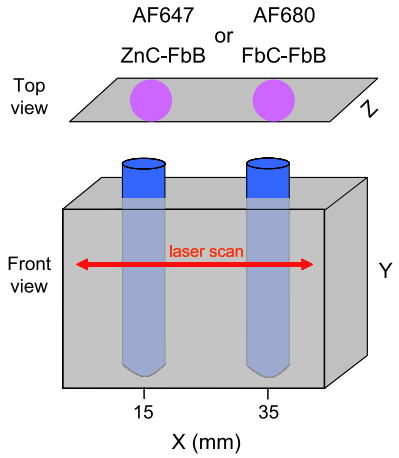

Figure 1. Schematic of the imaging experiment in which the two members of a pair of fluorophores (either **AF647** plus **AF680** or **ZnC-FbB** plus **FbC-FbB**) are placed at positions 15 or 35 mm in the *X* direction in an imaging tank containing optical index matching fluid. The laser (650 or 675 nm) is scanned in the *X* (horizontal) direction (0–50 mm), shifted in the *Y* (vertical) direction, and scanned again. The top (*X*–*Z*) view indicates schematically a typical 2D reconstruction of the fluorescence-intensity profile.

For each pair of dyads, excitation was provided by a diode laser at either 650 or 675 nm with a beam diameter at the sample of ~1 mm and a power adjusted to 3 mW. The fluorescence light passed through a 10 nm bandpass filter centered at either 700 or 760 nm. Thus, images derived from four excitation–detection pairs were obtained for each of the two pairs of samples, for a total of 16 individual images.

RESULTS AND DISCUSSION

Synthesis

The desired target compound **ZnC-FbB** was readily prepared by selective metalation of **FbC-FbB** (Scheme 1). The chlorin undergoes metalation with zinc acetate at room temperature whereas the bacteriochlorin fails to metalate under these conditions. The difficulties in metalating bacteriochlorins have been noted previously (58). Spectroscopic studies of the dyad **ZnC-FbB** required the availability of a benchmark chlorin containing the same set of substituents as those in the dyad. Thus, the free base chlorin **FbC1** was treated with zinc acetate to afford the corresponding zinc chelate **ZnC1** (Scheme 2).

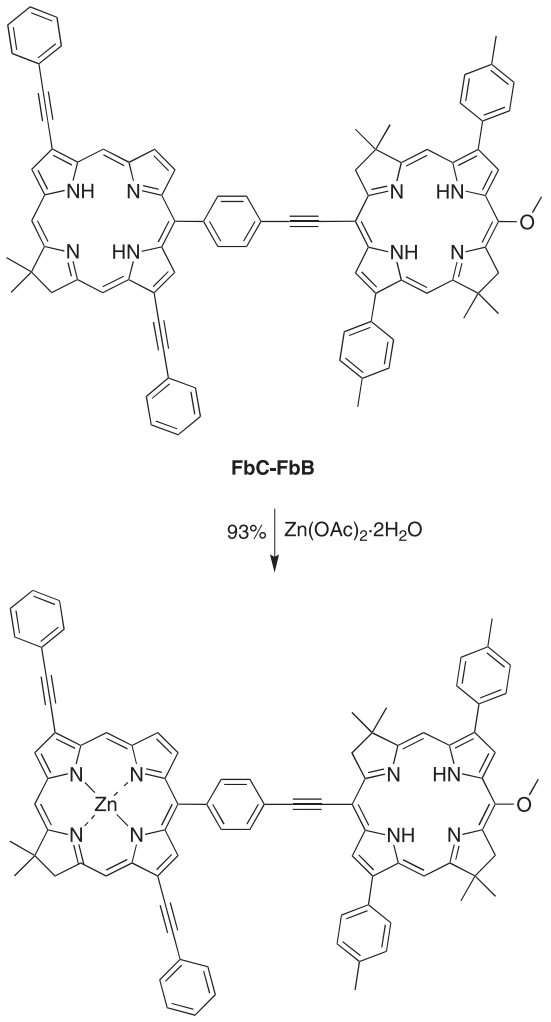

Scheme 1.

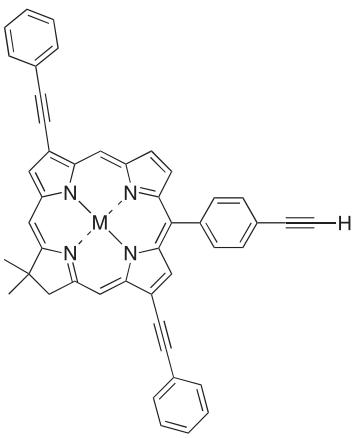

Scheme 2.

Chlorin–bacteriochlorin dyads in toluene

Figure 2 shows red- and NIR-region absorption and fluorescence spectra of **FbC-FbB** and benchmark monomers in toluene (53). The peak wavelengths and other key photophysical characteristics are summarized in Table 1. Figure 3 gives the analogous spectra obtained here for dyad **ZnC-FbB** in which the free base chlorin is replaced with its zinc chelate. The red (Q_y) band of the zinc chlorin has its absorption maximum at 650 nm, corresponding to a 110 nm shift from the bacteriochlorin fluorescence at 760 nm. Essentially no fluorescence is observed from the zinc chlorin (~655 nm) because energy transfer to the bacteriochlorin component is so efficient. The fluorescence quantum yield and singlet excited-state lifetime of the bacteriochlorin in **ZnC-FbB** (0.19, 5.3 ns) are essentially identical to those of the bacteriochlorin reference compound (0.19, 5.7 ns [53]), as is summarized in Table 1 for the samples in toluene.

Energy transfer from the zinc chlorin to the free base bacteriochlorin in **ZnC-FbB** was investigated using ultrafast transient absorption spectroscopy under the same conditions employed for **FbC-FbB**. In short, instantaneous bleaching of the zinc chlorin Q_y band at 675 nm decays and bleaching of the bacteriochlorin Q_y band at 760 nm grows with a time constant of 5.3 ± 0.2 ps. This value is assigned as the lifetime of the exited

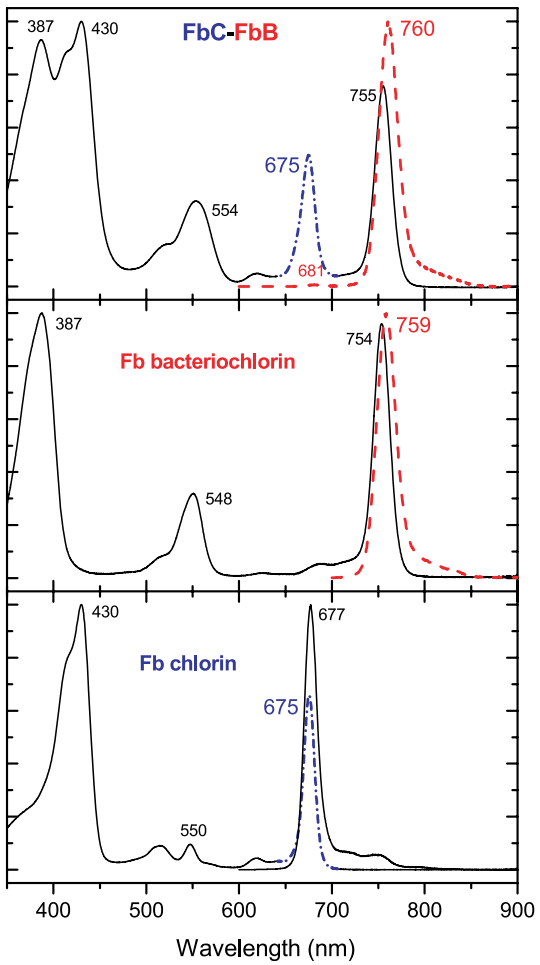

Figure 2. Spectra of chlorin–bacteriochlorin dyad **FbC-FbB** and constituents in toluene. $Q_y(0,0)$ absorption of the chlorin (dash-dot) and Q_y emission of the bacteriochlorin (dashed).

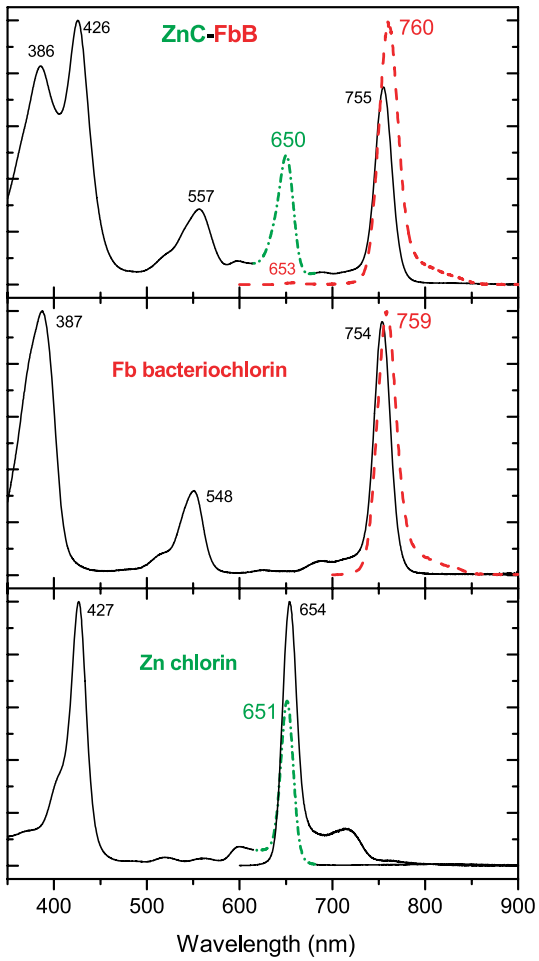

Figure 3. Spectra of chlorin–bacteriochlorin dyad **ZnC-FbB** and constituents in toluene. $Q_y(0,0)$ absorption of the chlorin (dash-dot) and Q_y emission of the bacteriochlorin (dashed).

singlet state of the zinc chlorin component of the dyad. This lifetime when compared with that for the benchmark monomeric zinc chlorin **ZnC1** gives a rate constant for energy transfer from the chlorin to bacteriochlorin of $k_{ENT} = (\tau_C^{dyad})^{-1} - (\tau_C^{mon})^{-1} = (5.3\,ps)^{-1} - (3.8\,ns)^{-1} \approx (5.3\,ps)^{-1}$. The energy-transfer yield is $\Phi_{ENT} = k_{ENT} \times \tau_C^{dyad} > 0.99$. Given that excitation energy transfer from chlorin to bacteriochlorin is rapid and effectively quantitative, **ZnC-FbB** behaves as though it is a single chromophore with an exceptionally large shift (110 nm) between the red chlorin absorption and the NIR bacteriochlorin fluorescence. This result is analogous to that for **FbC-FbB**, except in that case the absorption-fluorescence spacing is 85 nm (53).

Chlorin–bacteriochlorin dyads in DMSO

The photophysical characteristics of the two C–B dyads were also investigated in polar solvents. The details of these observations and analysis of the results will be reported elsewhere. Here we summarize key results in dimethylsulfoxide (DMSO) compared with toluene, which are the most and least polar solvents employed, respectively. On the basis of fluorescence yields, excited-state lifetimes and transient absorption studies, the yield of energy transfer from the excited chlorin to

bacteriochlorin remains very high (>90%) in the polar solvents. On the other hand, the fluorescence quantum yield of the bacteriochlorin in **FbC-FbB** is reduced from 0.19 in toluene (Table 1) to 0.019 in DMSO, and the singlet excited-state lifetime from 5.4 to 0.28 ns. For **FbC-FbB**, the bacteriochlorin fluorescence yield is reduced from 0.19 in toluene to 0.072 in DMSO, and the singlet excited-state lifetime from 5.3 to 2.4 ns. Thus, although the excited bacteriochlorin is quenched by 10-fold or more for **FbC-FbB** in DMSO relative to toluene, it is quenched by only about 2.5-fold for **ZnC-FbB**. These results are most consistent with the electron-transfer mechanism given in Eq. (1).

$$C - B^* \rightarrow C^- - B^+ \quad (1)$$

Here the excited bacteriochlorin (produced essentially quantitatively from the excited chlorin) undergoes electron transfer to give the reduced chlorin and the oxidized bacteriochlorin. This process is expected to be more energetically favorable than the formation of C^+–B^- because bacteriochlorins are more easily oxidized and harder to reduce than chlorins for a given metalation state (60). Given that zinc chlorins are harder to reduce than free base chlorins (42,59), the product state C^-–B^+ in Eq. (1) will be higher in energy for **ZnC-FbB** than in **FbC-FbB**, which underlies the substantial diminution of the quenching process in the dyad containing the zinc chorin.

Redox tuning of C–B dyads can be achieved by incorporation of electron-donating groups on the chlorin and/or electron-withdrawing groups on the bacteriochlorin. As with metalation, this approach to redox tuning is expected to destabilize the electron-transfer product and thereby suppress the intramolecular quenching reaction in polar media. We have previously demonstrated such redox tuning in porphyrins and chlorins (42,60). Such redox tuning is important for extension of analogs of the C–B dyads for use in aqueous media. On the other hand, in the absence of redox tuning, the quenching process in Eq. (1) and associated modulation of the fluorescence intensity and lifetime might be exploited as a probe of local polarity. Additionally, these dyads, like all imaging probes, may undergo intermolecular quenching energy- or electron-transfer reactions involving species present *in vivo*. Molecular designs for suppressing intermolecular aggregation of porphyrinic macrocycles in organic or aqueous media have been developed while retaining the intrinsic photophysical characteristics of the macrocycles (45–47,61–63).

Spectral comparison of chlorin–bacteriochlorin dyads and Alexa Fluor dyes

In the following, the spectral properties of two commercially available AF dyes (**AF647** and **AF680**) are compared with those of the two C–B dyads **FbC-FbB** and **ZnC-FbB**. The probes **AF647** and **AF680** were chosen from the list of available AF dyes to provide the closest match in absorption and fluorescence wavelengths with the two C–B dyads. Other choices of AF dyes would not have provided a viable comparison with the two C–B dyads or each other using two common excitation lasers and two common detection windows, given the spectral characteristics of the compounds. The absorption and fluorescence spectra of **AF647** and **AF680** in standard phosphate-buffered saline (PBS) solution are shown in Fig. 4, and key photophysical properties are listed in Table 1. The molar absorption coefficients were taken from the Invitrogen website (http://www.probes.invitrogen.com). The absorption and fluorescence positions, and fluorescence quantum yield and excited singlet-state lifetime (measured by fluorescence decay) were determined here. The absorption profiles (bandwidths) of the two AF dyes closely mimic those of the popular cyanine dyes Cy5 and Cy5.5 (28).

Several properties of the two AF dyes are superior to those of the chlorin and bacteriochlorin components of the dyads. For example, the peak molar absorption coefficients (ε) of the AF dyes are on the average three-fold greater than those of the chlorin components of the C–B dyads (and two-fold greater than those of the bacteriochlorin component). The fluorescence quantum yields (Φ_f) of the two AF dyes are about two-fold greater than that of the bacteriochlorin component of the dyads. The product $\varepsilon \times \Phi_f$ is a useful quantity in comparing probes for imaging applications and reflects the fluorescence intensity expected for a given probe concentration (absorption). The AF dyes have $\varepsilon \times \Phi_f$ values that are on the average six-fold higher than the dyads.

The advantage of the AF dyes expressed in the $\varepsilon \times \Phi_f$ parameter is greatly diminished when considering the two- to three-fold broader spectral features of these dyes when compared with those of the components of the C–B dyads (Table 1). This comparison is made in Figs. 5 and 6, which are normalized at the peak values to facilitate comparison of the spectral shapes. Figures 5 and 6 also indicate the two absorption wavelengths (650 and 675 nm) and the two 10 nm wide fluorescence windows (centered at 700 and 760 nm) used in the

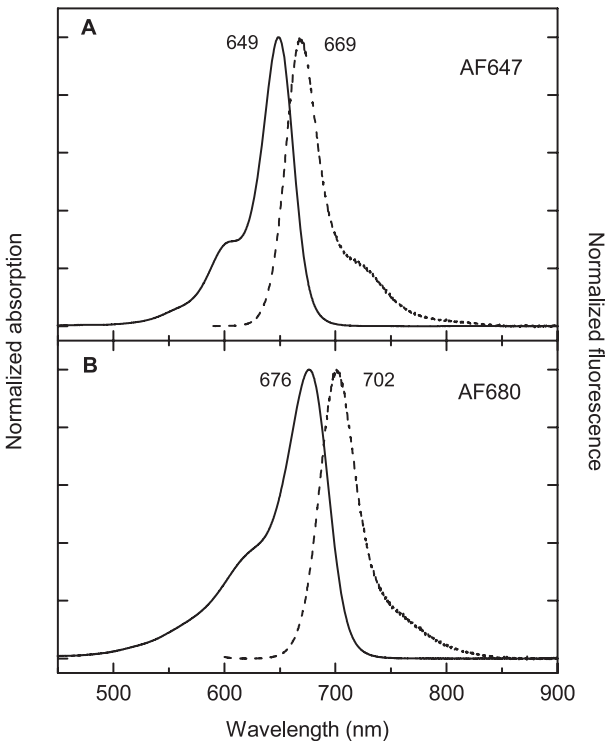

Figure 4. Absorption and fluorescence spectra of two commercially available Alexa Fluor dyes in PBS. The peak wavelengths (nm) are indicated.

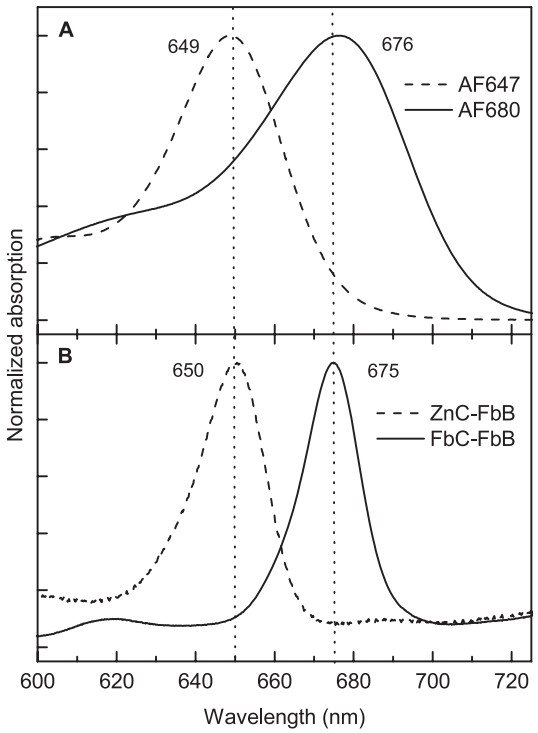

Figure 5. Red-region absorption spectra of (A) Alexa Fluor dyes in PBS and (B) chlorin–bacteriochlorin dyads in toluene. The peak absorption and emission wavelengths (nm) are denoted. The dashed vertical lines indicate the two wavelengths of excitation (650 and 675 nm) used for imaging studies on phantoms.

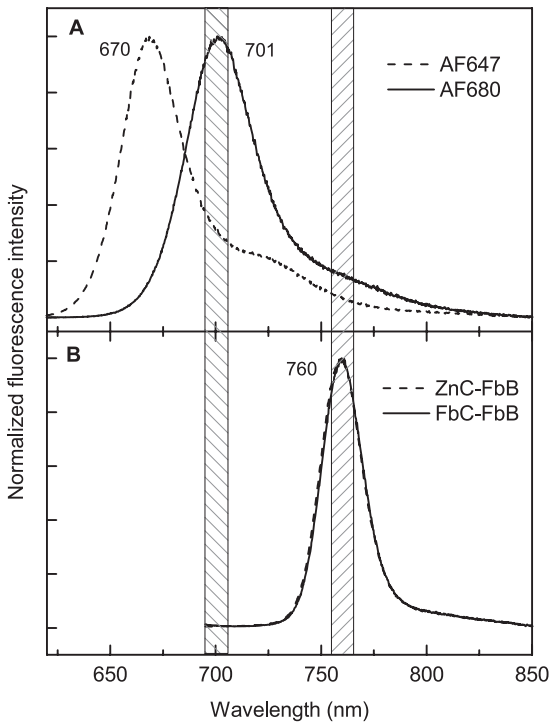

Figure 6. NIR fluorescence spectra of (A) Alexa Fluor dyes in PBS and (B) chlorin–bacteriochlorin dyads in toluene. The peak emission maxima (nm) are denoted. The hashed slices indicate the two 10 nm bandpass detection windows centered at 700 and 760 nm utilized in imaging studies on phantoms.

imaging studies described below. The broad spectral features affect the ability to use simultaneously more than one optical probe.

Consider an application wherein it is desirable to utilize two optical probes. One application may involve targeting to a given locale (cell, organelle, *etc*.) to enhance contrast *via* simultaneous (coincidence) detection of fluorescence (intensity in this example) of the two probes. Another application may involve simultaneous detection of two probes targeted to different sites to capture the two sites in the same image. Consider first the relative absorption spectral characteristics of the two classes of compounds (Fig. 5). Essentially exclusive (>90%) excitation of the zinc chlorin of **ZnC-FbB** at 650 nm or the free base chlorin of **FbC-FbB** at 675 nm can be achieved if both dyads are present due to the narrow spectral widths and thus good separation between the absorption features (Fig. 5B). On the other hand, if both of the AF dyes were present, excitation at 650 nm, at the absorption peak for **AF647**, will result in about 30% of the excitation light being absorbed by **AF680** due to the large breadths of the features, most notably the strong shoulder on the short-wavelength side of the **AF680** band (Fig. 5A). Excitation would be more selective for **AF680** near its absorption maximum. Collectively, these comparisons suggest that even though the molar absorption coefficients of the AF dyes are greater, more selective excitation (and thus imaging) can be attained for the C–B dyads based on the absorption characteristics.

Consider next the comparative fluorescence properties (Fig. 6). The 10 nm slices shown on this figure represent the bandpass of the interference filters used in the imaging studies of these compounds described below. The feature shown in Fig. 6B is the fluorescence observed from the free base bacteriochlorin component common to both **ZnC-FbB** and **FbC-FbB**. Because the spectra in these figures are normalized to facilitate comparisons, the area under the 10 nm wide rectangular collection window centered at 760 nm has a value of 10. The integrated intensity of the total bacteriochlorin fluorescence has a value of 29. Thus, 30% of the total fluorescence from this dyad probe would be collected using this detection window. By contrast, a 10 nm collection window centered at 700 nm (area of 10) for **AF680** would collect only 20% of the total fluorescence from that compound (which has an integrated value of 51). If that same window were used to collect emission from **AF680**, only 6% of the emission from that compound would be collected. Furthermore, if selectivity of detection were an issue, probing with a 10 nm bandpass at 700 nm would give substantial signals from both AF dyes. On the other hand, if two C–B dyads were used that had different bacteriochlorin acceptors with peaks having the same 30 nm separation as for the AF dyes, selective (>90%) detection of one probe in the presence of the other could be achieved due to the narrow bandwidths.

In summary, although the two AF dyes have on average six-fold larger $\varepsilon \times \Phi_f$ values than the C–B dyads, a factor of 1.5 of that value is lost even under the most optimal detection condition, namely detection at the fluorescence peak of the dye (*e.g.* at 700 nm for **AF680**), and the entire advantage factor can be lost for detection off the peak but still within the major part of the broad emission (*e.g.* at 700 nm for **AF647**). In this regard, off-resonance detection using the broad long-wavelength side of the emission is commonly utilized with these

types of dyes, to achieve a sufficiently large absorption–emission shift to minimize scattered excitation light reaching the detector. This is necessary because the absorption and fluorescence maxima are only separated by 20–30 nm (Fig. 3). Similarly, excitation on the shorter-wavelength side of the broad absorption feature is often used for the same reason. Such off-resonance excitation or detection reduces any advantage (compared to another probe) of a large peak molar absorption coefficient because the maximum possible number of photons that could be absorbed by the probe are not actually captured. The use of such off-resonance detection to gain a large absorption-fluorescence spacing is not necessary for the chlorin–bacteriochlorin dyads due to the very large effective Stokes shifts (85 or 110 nm for **FbC-FbB** or **ZnC-FbB**, respectively). Thus, both excitation and detection can be made at the absorption and fluorescence maxima, making full use of the absorption and fluorescence capabilities of the components utilized in the energy-transfer construct. It is further anticipated that excellent selectivity can be achieved (in both excitation and detection) if two or more C–B probes are present. To explore these issues, imaging studies using phantoms were carried out.

Imaging studies of chlorin–bacteriochlorin dyads and Alexa Fluor dyes

To establish the performance of these dyes in the context of diffuse imaging, imaging studies of the pair of C–B dyads (**FbC-FbB** and **ZnC-FbB**) were performed with the small animal diffuse optical tomography system. For comparison, images were also acquired for the pair of AF dyes (**AF647** and **AF680**). For each dye pair, excitation was at either 650 or 675 nm (laser diodes at 3 mW) and detection was at either 700 or 760 nm (10 nm bandpass). These excitation and detection conditions are illustrated schematically on the spectral features of the compounds in Figs. 5 and 6. Typical image reconstructions using the *X*–*Z* view are given in Fig. 7 for the two C–B dyads. In the top panel, excitation at 650 nm and detection at 760 nm was used, and for the bottom panel excitation at 675 nm and detection at 760 nm was employed. In both cases, dyad **ZnC-FbB** was mounted in the chamber at position 15 mm in the *X* (horizontal) direction and dyad **FbC-FbB** was mounted at position 35 mm. Similar runs were performed for the two C–B dyads using 700 nm detection, and for the two AF dyes using the combinations of 650 or 675 nm excitation and 700 or 760 nm detection.

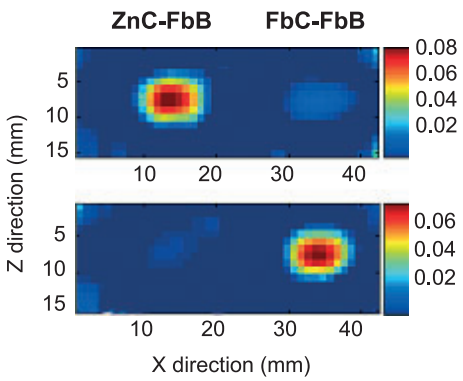

Figure 7. Illustrative *X*–*Z* (top view) slice from a 2D tomographic reconstruction of tissue-like phantoms consisting of chlorin–bacteriochlorin dyads (1 μM) in 3 mm inner diameter glass tubes. The two phantoms were at positions 15 mm (**ZnC-FbB**) and 35 mm (**FbC-FbB**) in the *X* direction (and centered in the *Z* direction) in an imaging tank containing optical matching fluid. Top panel: 650 nm excitation. Bottom panel: 675 nm excitation. In both experiments, the fluorescence was collected through a narrow bandpass filter (760 nm, FWHM 10 nm). See Fig. 1 for a layout of the experiment.

Figure 8 focuses on the respective image for each compound for each excitation/detection combination. The value above each image gives the fluorescence counts obtained by integrating a 4 mm wide by 3 mm high region centered on the position where the laser illuminated the sample tube. This quantitation was carried out to minimize counts arising from (1) light scattering off of the walls of the tube and (2) background counts from regions having significantly reduced light signal levels compared to the maximum (*i.e.* in the index-matching fluid outside the sample). Below, we focus mainly on qualitative characteristics that can be obtained from Fig. 8.

The images are somewhat brighter for the AF dyes than for the dyads for excitation or detection near the peak wavelengths, as is expected given the photophysical characteristics described above (Figs. 5 and 6 and Table 1). For example, excitation of **AF680** at 675 nm and detection at 700 nm (near the peak wavelengths; Figs. 5A and 6A) produces an image with a maximum intensity of ~0.2 (Fig. 8P), whereas excitation of **ZnC-FbB** at 650 nm and detection at 760 nm (near the peak wavelengths; Figs. 5B and 6B) gives an image with an intensity of ~0.07, about three times smaller (Fig. 8A). A similar comparison was obtained upon detection at 700 nm for **AF647** with excitation at 650 nm (Fig. 8M) and **AF680** with excitation at 675 nm (Fig. 8P), which in both cases is near the respective absorption maximum (Fig. 5A). The image for **AF647** is weaker than that for **AF680** even though the former has a 30% greater molar absorption coefficient and a comparable fluorescence yield (Table 1) because the 700 nm detection window rests on the long-wavelength shoulder of the **AF647** emission, down about 70% from the peak value (Fig. 6A). Finally, the result given above for **ZnC-FbB** using excitation (650 nm) and detection (760 nm) at its peak wavelengths can be compared with that for **FbC-FbB** using excitation (675 nm) and detection (760 nm) at its peak wavelengths (Figs. 5B and 6B). The relevant images are given in Fig. 8A,D, respectively. Within experimental uncertainty, the differences observed in these pair-wise comparisons are consistent with the respective differences in spectral profiles, molar absorption coefficients, fluorescence quantum yields and fraction of the fluorescence profile encompassed by the 10 nm detection window.

The two AF dyes give somewhat (up to three-fold) brighter images than the C–B dyads when the absorption and detection wavelengths are chosen at the optimum spectral positions; however, the AF dyes give poor excitation and detection selectivity compared to the C–B dyads. This result was anticipated on the basis of the spectra described above (Figs. 5 and 6). The C–B dyads give excellent discrimination as can be seen on Fig. 8A–D (760 nm detection), for which two panels on the diagonal should be bright and those on the off-diagonal should be dark. Similarly, Fig. 8E–H (700 nm detection) should be dark because essentially no emission occurs from the chlorin due to the high yield of energy transfer to the bacteriochlorin component of the dyads. For example,

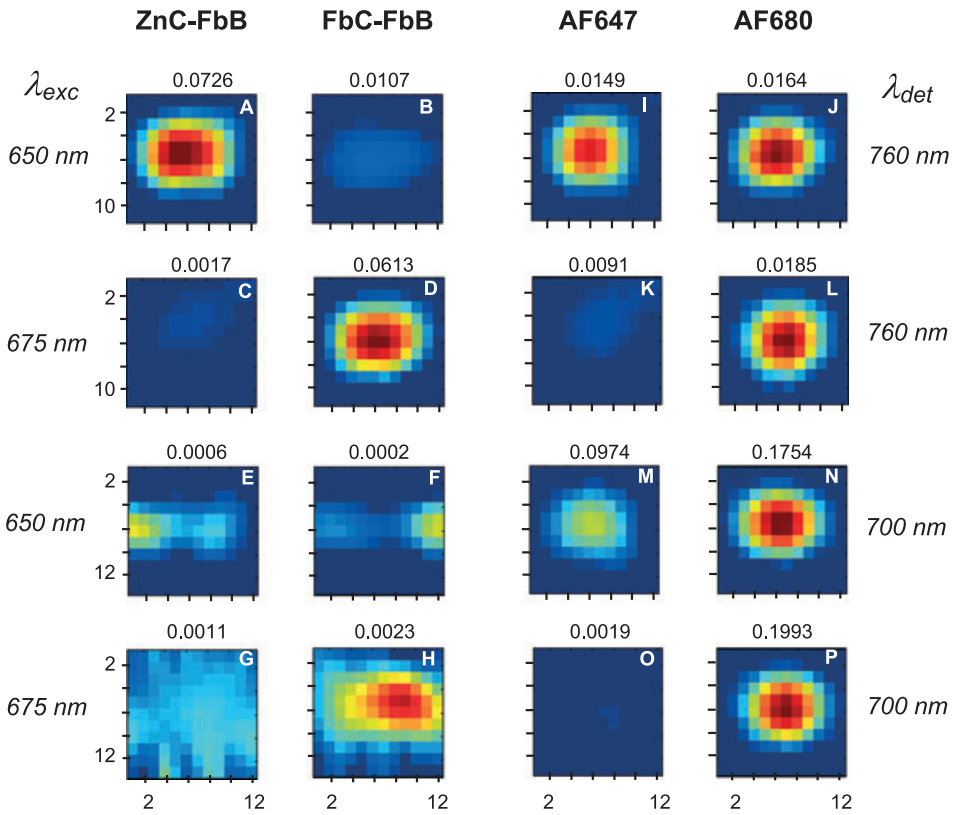

Figure 8. Reconstructed images encompassing a 3 mm (pixels 4–7 on the vertical axis [*Z* direction in Fig. 7]) by 4 mm wide (pixels 4–8 on the horizontal axis [*X* direction in Fig. 7]) region centered on the brightest spot in each image. See Fig. 7 for the original images that give rise to images (A)–(D) here. The value listed above each image is the mean value of the fluorescence (plus background) counts in that window. The same color intensity scale is used for all panels.

Fig. 8A,D (discussed above) gives images for excitation of the **ZnC-FbB** or **FbC-FbB** at the chlorin absorption maximum and detection at the bacteriochlorin fluorescence maximum. These images are bright. For perfect selectivity, the images in Fig. 8B,C would have no intensity. This optimum condition is effectively met, as the mean intensities in Fig. 8B,C are about 17% and 2% of the values in Fig. 8D,A, respectively. The intensity slightly above the noise floor in Fig. 8B arises because of small (2% of the peak value) absorption for **FbC-FbB** on the higher-energy side of the $Q_y(0,0)$ maximum leading into the weak $Q_y(1,0)$ vibronic satellite at ~620 nm (Fig. 5B). The additional criterion for perfect selectivity for the C–B dyads would be that the images in Fig. 8E–H are dark. This condition is effectively met because the maximum intensity in any of the panels is only 3% of that in Fig. 8D,A, and is < 1% in two of the panels. That the intensity is not simply at the noise level arises because there is a small (≤1%) fluorescence from the chlorin unit competing with the ≥99% yield of energy transfer to the bacteriochlorin unit.

The excellent selectivity for the C–B dyads stands in contrast to the findings for the AF dyes. For example, Fig. 8M–P for the AF dyes can be compared with the analogs for the C–B dyads discussed above (Fig. 8A–D). In particular, for good selectivity, there should be no intensity in Fig. 8N; however, the value is about 85% of that of Fig. 8P. This result arises because of the extremely broad absorption contour for **AF680** (Fig. 5A). Similarly, the images in Fig. 8I–L should be dark for the AF dyes, but in three cases (Fig. 8I,J,L) the levels are 10–15% of the maximal cases (Fig. 8M,N,P). The latter arise due to the broad emission profiles for the AF dyes, which allow capturing intensity even if the detection windows are displaced by 60 nm (760 *versus* 700 nm).

One limitation of the comparisons made above is that the properties of the C–B dyads are being contrasted with those of monomeric AF dyes. Some improvement in the attributes are expected with a fictive dyad of **AF647** and **AF680** (or two other AF dyes) assuming quantitative intramolecular energy transfer. Nonetheless, the advantages of the C–B dyads compared to such constructs of AF dyes or other fluorophores with similarly broad spectral features would be retained. The ability to selectively excite and selectively detect one probe in the presence of the other, and the number of detection windows available within a given spectral window will always be enhanced by the use of probes (regardless of monomeric or dyad constructs) that exhibit narrow spectral features.

OUTLOOK

The two C–B dyads examined herein are prototypes of a possible new class of optical imaging probes. The dyads are characterized by narrow absorption and emission bandwidths (~20 nm), a reasonably strong molar absorption coefficient of the chlorin (donor), fast and nearly quantitative energy transfer to the bacteriochlorin (acceptor), modest fluorescence emission intensity and long fluorescence lifetime of the bacteriochlorin, and an extremely large (85 or 110 nm)

absorption-fluorescence spacing. While the molar absorption coefficient and the fluorescence intensity are only modest, the combined features of the energy-transfer dyads are quite attractive. The narrow absorption band enables selective excitation, whereas the narrow emission band ensures that a very large percentage of the emission can be collected in a narrow detection channel. Together, the narrow bands should enable multicolor applications wherein a number of similar probes could be used in concert with a high rejection of inter-probe cross talk. The large absorption-fluorescence spacing minimizes stray excitation light from reaching the detection monochromator. On the basis of the comparisons made herein, water-soluble C–B dyads having the same spectral and photophysical attributes are expected to afford superior features to cyanine dyes (including the AF series) or other probes that are characterized by broad absorption and emission profiles.

A sizable number of chlorin and bacteriochlorin building blocks are known whose absorption encompasses the entire spectral region from 600 to 750 nm, with similar coverage in fluorescence wavelengths (past 800 nm) (41,42,44,45). Accordingly, independent tuning of the energy donor and acceptor subunits in chlorin- and bacteriochlorin-based dyads may afford families of probes that have spectral properties (absorption and fluorescence wavelengths and spacing) and fluorescence lifetimes that match the requirements of specific molecular-imaging applications. Through use of the building blocks, a cassette of dyads can be envisaged that utilize the same donor (for excitation at the same laser wavelength) and different acceptor bacteriochlorins (for detection in different fluorescence channels). Combinations with other red or NIR chromophores (64,65) are also possible. The resulting selectivity is expected to afford a much larger number of detection channels in a given range for multicolor applications. These include targeting a given locale (cell, organelle, *etc*.) with two probes and then using simultaneous (coincidence) detection of the fluorescence (spectra) from both probes to increase contrast over the background. Similarly, the use of two probes targeting different sites to interrogate different cell/tissue disease states or functions would be more efficacious with enhanced probe excitation/detection selectivity.

In addition to intensity-based measurements, the dyads containing chlorin or bacteriochlorin components may be quite attractive for lifetime imaging applications. For example, the singlet excited-state (fluorescence) lifetime is ~5 ns for the bacteriochlorin subunit in the two dyads investigated here in polar media, although in polar media the lifetime is significantly shorter for **FbC-FbB** and modestly (up to two-fold) shorter for **ZnC-FbB** owing to intramolecular electron-transfer quenching. In contrast, the lifetime is 1.2 or 1.4 ns for the two AF dyes investigated (Table 1). Lifetimes on the order of 1 ns are in the range of the largest lifetime background signals found in many *in vivo* applications; dyes with lifetimes in this regime will give less than optimal contrast. The bacteriochlorins studied here would be expected to give greater contrast if redox tuning can be exploited to suppress intramolecular quenching processes and thereby retain lifetimes of up to 5 ns. The use of other central metal ions will allow tuning down to the picosecond range if desired. Thus, the tunable lifetimes that can be attained with bacteriochlorins may be quite attractive for multiprobe applications employing lifetime detection. Further advantages in selectivity of detection and contrast can be envisaged by combining imaging criteria based on simultaneous fluorescence spectral and lifetime acquisition protocols.

The use of C–B dyads of the type described herein for *in vivo* applications requires provisions for water solubilization and bioconjugation. Achieving high water solubility is essential, given that a probe with excellent photophysical features may be rendered ineffective for optical imaging if poor aqueous solubility results in aggregation *in vivo*, whereupon low fluorescence may be observed and persistence in nontarget organs may result in unwanted and prolonged photosensitivity. Strategies for imparting water solubility to tetrapyrrole macrocycles are known (46,47,62,63), yet water-soluble dyads have not yet been prepared. In many respects the present synthetic chemistry capabilities for chlorins and bacteriochlorins resemble that of cyanine dyes in the 1980s. The extension of the present results to obtain water-soluble bioconjugatable C–B dyads would appear to open new opportunities in NIR imaging, particularly where probes for multicolor or multi-lifetime applications are desired.

Acknowledgements—This research was supported by grants from the Division of Chemical Sciences, Geosciences and Biosciences Division, Office of Basic Energy Sciences, Office of Science, U.S. Department of Energy to D.H. (DE-FG02-05ER15661), D.F.B. (DE-FG02-05ER15660) and J.S.L. (DE-FG02-96ER14632) and a grant from the National Institutes of Health to J.P.C. (K25-NS44339). In addition, J.P.C. received support from grants BRG R01 CA109754 and SAIRP R24 CA83060 from the National Institutes of Health. H.L.K. was supported by the Imaging Sciences Pathway training grant from the NIH (5T90 DA022871) at Washington University. Mass spectra were obtained at the Mass Spectrometry Laboratory for Biotechnology at North Carolina State University. Partial funding for the Facility was obtained from the North Carolina Biotechnology Center and the National Science Foundation.

REFERENCES

1. Weissleder, R. and M. J. Pittet (2008) Imaging in the era of molecular oncology. *Nature* **452**, 580–589.
2. Klohs, J., A. Wunder and K. Licha (2008) Near-infrared fluorescent probes for imaging vascular pathophysiology. *Basic Res. Cardiol.* **103**, 144–151.
3. Wessels, J. T., A. C. Busse, J. Mahrt, C. Dullin, E. Grabbe and G. A. Mueller (2007) In vivo imaging in experimental preclinical tumor research–A review. *Cytometry* **71A**, 542–549.
4. Rao, J., A. Dragulescu-Andrasi and H. Yao (2007) Fluorescence imaging *in vivo*: Recent advances. *Curr. Opin. Biotechnol.* **18**, 17–25.
5. Licha, K. and C. Olbrich (2007) Optical imaging in drug discovery and diagnostic applications. *Adv. Drug Deliv. Rev.* **57**, 1087–1108.
6. Neves, A. A. and K. M. Brindle (2006) Assessing responses to cancer therapy using molecular imaging. *Biochim. Biophys. Acta* **1766**, 242–261.
7. Ballou, B., L. A. Ernst and A. S. Waggoner (2005) Fluorescence imaging of tumors *in vivo*. *Curr. Med. Chem.* **12**, 795–805.
8. Becker, W., A. Bergmann, G. Biscotti and A. Rueck (2004) Advanced time-correlated single photon counting techniques for spectroscopy and imaging in biomedical systems. *Proc. SPIE* **5340**, 104–112.
9. Achilefu, S. (2004) Lighting up tumors with receptor-specific optical molecular probes. *Technol. Cancer Res. Treat.* **3**, 393–409.
10. Gurfinkel, M., S. Ke, X. Wen, C. Li and E. M. Sevick-Muraca (2003, 2004) Near-infrared fluorescence optical imaging and tomography. *Dis. Markers* **19**, 107–121.

11. Gandjbakhche, A. H., V. Chernomordik, D. Hattery, M. Hassan and I. Gannot (2003) Tissue characterization by quantitative optical imaging methods. *Technol. Cancer Res. Treat.* **2**, 537–551.
12. Gratton, E., S. Breusegem, J. Sutin, Q. Ruan and N. Barry (2003) Fluorescence lifetime imaging for the two-photon microscope: Time-domain and frequency-domain methods. *J. Biomed. Opt.* **8**, 381–390.
13. Licha, K. (2002) Contrast agents for optical imaging. *Top. Curr. Chem.* **222**, 1–29.
14. Weissleder, R. and U. Mahmood (2001) Molecular imaging—Special review. *Radiology* **219**, 316–333.
15. Hawrysz, D. J. and E. M. Sevick-Muraca (2000) Developments toward diagnostic breast cancer imaging using near-infrared optical measurements and fluorescent contrast agents. *Neoplasia* **2**, 388–417.
16. Squire, A., P. J. Verveer and P. I. H. Bastiaens (2000) Multiple frequency fluorescence lifetime imaging microscopy. *J. Microsc.* **197**, 136–149.
17. Doja, M. Q. (1931) The cyanine dyes. *Chem. Rev.* **11**, 273–321.
18. Hamer, F. M. (1964) *The Cyanine Dyes and Related Compounds*. Wiley and Sons, New York.
19. Sturmer, D. M. and D. W. Heseltine (1977) Sensitizing and desensitizing dyes. In *The Theory of the Photographic Process*, 4th edn (Edited by T. H. James), pp. 194–234. Macmillan Publishing Co., Inc., New York.
20. Ernst, L. A., R. K. Gupta, R. B. Mujumdar and A. S. Waggoner (1989) Cyanine dye labeling reagents for sulfhydryl groups. *Cytometry* **10**, 3–10.
21. Mujumdar, R. B., L. A. Ernst, S. R. Mujumdar and A. S. Waggoner (1989) Cyanine dye labeling reagents containing isothiocyanate groups. *Cytometry* **10**, 11–19.
22. Southwick, P. L., L. A. Ernst, E. W. Tauriello, S. R. Parker, R. B. Mujumdar, S. R. Mujumdar, H. A. Clever and A. S. Waggoner (1990) Cyanine dye labeling reagents—Carboxymethylindocyanine succinimidyl esters. *Cytometry* **11**, 418–430.
23. Mujumdar, R. B., L. A. Ernst, S. R. Mujumdar, C. J. Lewis and A. S. Waggoner (1993) Cyanine dye labeling reagents: Sulfoindocyanine succinimidyl esters. *Bioconjugate Chem.* **4**, 105–111.
24. Mujumdar, S. R., R. B. Mujumdar, C. M. Grant and A. S. Waggoner (1996) Cyanine-labeling reagents: Sulfobenzindocyanine succinimidyl esters. *Bioconjugate Chem.* **7**, 356–362.
25. Tsien, R. Y., L. Ernst and A. Waggoner (2006) Fluorophores for confocal microscopy: Photophysics and photochemistry. In *Handbook of Biological Confocal Microscopy*, 3rd edn (Edited by J. B. Pawley), pp. 338–352. Springer Science + Business Media, New York.
26. Akers, W., F. Lesage, D. Holten and S. Achilefu (2007) In vivo resolution of multiexponential decays of multiple near-infrared molecular probes by fluorescence lifetime-gated whole-body time-resolved diffuse optical imaging. *Mol. Imaging* **6**, 237–246.
27. Panchuk-Voloshina, N., R. P. Haugland, J. Bishop-Stewart, M. K. Bhalgat, P. J. Millard, F. Mao, W.-Y. Leung and R. P. Haugland (1999) Alexa dyes, a series of new fluorescent dyes that yield exceptionally bright, photostable conjugates. *J. Histochem. Cytochem.* **47**, 1179–1188.
28. Berlier, J. E., A. Rothe, G. Buller, J. Bradford, D. R. Gray, B. J. Filanoski, W. G. Telford, S. Yue, J. Liu, C.-Y. Cheung, W. Chang, J. D. Hirsch, J. M. Beechem, R. P. Haugland and R. P. Haugland (2003) Quantitative comparison of long-wavelength Alexa Fluor dyes to Cy dyes: Fluorescence of the dyes and their bioconjugates. *J. Histochem. Cytochem.* **51**, 1699–1712.
29. Mishra, A., R. K. Behera, P. K. Behera, B. K. Mishra and G. B. Behera (2000) Cyanines during the 1990s: A review. *Chem. Rev.* **100**, 1973–2011.
30. Hilderbrand, S. A., K. A. Kelly, R. Weissleder and C.-H. Tung (2005) Monofunctional near-infrared fluorochromes for imaging applications. *Bioconjugate Chem.* **16**, 1275–1281.
31. Perlitz, C., K. Licha, F.-D. Scholle, B. Ebert, M. Bahner, P. Hauff, K. T. Moesta and M. Schirner (2005) Comparison of two tricarbocyanine-based dyes for fluorescence optical imaging. *J. Fluor.* **15**, 443–454.
32. Pham, W., Z. Medarova and A. Moore (2005) Synthesis and application of a water-soluble near-infrared dye for cancer detection using optical imaging. *Bioconjugate Chem.* **16**, 735–740.
33. Kobayashi, M., M. Akiyama, H. Kano and H. Kise (2006) Spectroscopy and structure determination. In *Chlorophylls and Bacteriochlorophylls: Biochemistry, Biophysics, Functions and Applications* (Edited by B. Grimm, R. J. Porra, W. Rüdiger and H. Scheer), pp. 79–94. Springer, Dordrecht, The Netherlands.
34. Pandey, R. K., L. N. Goswami, Y. Chen, A. Gryshuk, J. R. Missert, A. Oseroff and T. J. Dougherty (2006) Nature: A rich source for developing multifunctional agents. Tumor-imaging and photodynamic therapy. *Lasers Surg. Med.* **38**, 445–467.
35. Chen, Y., G. Li and R. K. Pandey (2004) Synthesis of bacteriochlorins and their potential utility in photodynamic therapy (PDT). *Curr. Org. Chem.* **8**, 1105–1134.
36. Limantara, L., P. Koehler, B. Wilhelm, R. J. Porra and H. Scheer (2006) Photostability of bacteriochlorophyll *a* and derivatives: Potential sensitizers for photodynamic tumor therapy. *Photochem. Photobiol.* **82**, 770–780.
37. Kozyrev, A. N., Y. Chen, L. N. Goswami, W. A. Tabaczynski and R. K. Pandey (2006) Characterization of porphyrins, chlorins, and bacteriochlorins formed via allomerization of bacteriochlorophyll *a*. Synthesis of highly stable bacteriopurpurinimides and their metal complexes. *J. Org. Chem.* **71**, 1949–1960.
38. Ptaszek, M., B. E. McDowell, M. Taniguchi, H.-J. Kim and J. S. Lindsey (2007) Sparsely substituted chlorins as core constructs in chlorophyll analogue chemistry. Part 1: Synthesis. *Tetrahedron* **63**, 3826–3839.
39. Taniguchi, M., M. Ptaszek, B. E. McDowell and J. S. Lindsey (2007) Sparsely substituted chlorins as core constructs in chlorophyll analogue chemistry. Part 2: Derivatization. *Tetrahedron* **63**, 3840–3849.
40. Taniguchi, M., M. Ptaszek, B. E. McDowell, P. D. Boyle and J. S. Lindsey (2007) Sparsely substituted chlorins as core constructs in chlorophyll analogue chemistry. Part 3: Spectral and structural properties. *Tetrahedron* **63**, 3850–3863.
41. Kee, H. L., C. Kirmaier, Q. Tang, J. R. Diers, C. Muthiah, M. Taniguchi, J. K. Laha, M. Ptaszek, J. S. Lindsey, D. F. Bocian and D. Holten (2007) Effects of substituents on synthetic analogs of chlorophylls. Part 1: Synthesis, vibrational properties and excited-state decay characteristics. *Photochem. Photobiol.* **83**, 1110–1124.
42. Kee, H. L., C. Kirmaier, Q. Tang, J. R. Diers, C. Muthiah, M. Taniguchi, J. K. Laha, M. Ptaszek, J. S. Lindsey, D. F. Bocian and D. Holten (2007) Effects of substituents on synthetic analogs of chlorophylls. Part 2: Redox properties, optical spectra and electronic structure. *Photochem. Photobiol.* **83**, 1125–1143.
43. Kim, H.-J. and J. S. Lindsey (2005) De novo synthesis of stable tetrahydroporphyrinic macrocycles: Bacteriochlorins and a tetradehydrocorrin. *J. Org. Chem.* **70**, 5475–5486.
44. Taniguchi, M., D. L. Cramer, A. D. Bhise, H. L. Kee, D. F. Bocian, D. Holten and J. S. Lindsey (2008) Accessing the near-infrared spectral region with stable, synthetic, wavelength-tunable bacteriochlorins. *New J. Chem.* **32**, 947–958.
45. Borbas, K. E., C. Ruzié and J. S. Lindsey (2008) Swallowtail bacteriochlorins. Lipophilic absorbers for the near-infrared. *Org. Lett.* **10**, 1931–1934.
46. Borbas, K. E., V. Chandrashaker, C. Muthiah, H. L. Kee, D. Holten and J. S. Lindsey (2008) Design, synthesis, and photophysical characterization of water-soluble chlorins. *J. Org. Chem.* **73**, 3145–3158.
47. Ruzié, C., M. Krayer, T. Balasubramanian and J. S. Lindsey (2008) Tailoring a bacteriochlorin building block with cationic, amphipathic, or lipophilic substituents. *J. Org. Chem.* **73**, 5806–5820.
48. Beavis, A. J. and K. J. Pennline (1996) Allo-7: A new fluorescent tandem dye for use in flow cytometry. *Cytometry* **24**, 390–394.
49. Roederer, M., A. B. Kantor, D. R. Parks and L. A. Herzenberg (1996) Cy7PE and Cy7APC: Bright new probes for immunofluorescence. *Cytometry* **24**, 191–197.
50. Roederer, M., S. De Rosa, R. Gerstein, M. Anderson, M. Bigos, R. Stovel, T. Nozaki, D. Parks, L. Herzenberg and L. Herzenberg (1997) 8 Color, 10-parameter flow cytometry to elucidate complex leukocyte heterogeneity. *Cytometry* **29**, 328–339.
51. Harvey, P. D. (2003) Recent advances in free and metalated multiporphyrin assemblies and arrays; a photophysical behavior and energy transfer perspective. In *The Porphyrin Handbook*,

Vol. 18 (Edited by K. M. Kadish, K. M. Smith and R. Guilard), pp. 63–250. Academic Press, San Diego.
52. Holten, D., D. F. Bocian and J. S. Lindsey (2002) Probing electronic communication in multiporphyrin arrays. A guide to the rational design of molecular photonic devices. *Acc. Chem. Res.* **35**, 57–69.
53. Muthiah, C., H. L. Kee, J. R. Diers, D. Fan, M. Ptaszek, D. F. Bocian, D. Holten and J. S. Lindsey (2008) Synthesis and excited-state photodynamics of a chlorin–bacteriochlorin dyad—Through-space versus through-bond energy transfer in tetrapyrrole arrays. *Photochem. Photobiol.* **84**, 786–801.
54. Patwardhan, S. V., S. R. Bloch, S. Achilefu and J. P. Culver (2005) Time-dependent whole-body fluorescence tomography of probe bio-distributions in mice. *Opt. Express* **13**, 2564–2577.
55. Pogue, B. W. and M. S. Patterson (2006) Review of tissue simulating phantoms for optical spectroscopy, imaging and dosimetry. *J. Biomed. Opt.* **11**, 041102-1–041102-16.
56. Weber, G. and F. W. J. Teale (1957) Determination of the absolute quantum yield of fluorescent solutions. *Trans. Faraday Soc.* **53**, 646–655.
57. Gradyushko, A. T., A. N. Sevchenko, K. N. Solovyov and M. P. Tsvirko (1970) Energetics of photophysical processes in chlorophyll-like molecules. *Photochem. Photobiol.* **11**, 387–400.
58. Hartwich, G., L. Fiedor, I. Simonin, E. Cmiel, W. Schäfer, D. Noy, A. Scherz and H. Scheer (1998) Metal-substituted bacteriochlorophylls. 1. Preparation and influence of metal and coordination on spectra. *J. Am. Chem. Soc.* **120**, 3675–3683.
59. Felton, R. H. (1978) Primary redox reactions of metalloporphyrins. In *The Porphyrins*, Vol. 5 (Edited by D. Dolphin), pp. 53–125. Academic Press, New York.
60. Yang, S. I., J. Seth, J.-P. Strachan, S. Gentemann, D. Kim, D. Holten, J. S. Lindsey and D. F. Bocian (1999) Ground and excited state electronic properties of halogenated tetraarylporphyrins. Tuning the building blocks for porphyrin-based photonic devices. *J. Porphyrins Phthalocyanines* **3**, 117–147.
61. Thamyongkit, P., M. Speckbacher, J. R. Diers, H. L. Kee, C. Kirmaier, D. Holten, D. F. Bocian and J. S. Lindsey (2004) Swallowtail porphyrins: Synthesis, characterization and incorporation into porphyrin dyads. *J. Org. Chem.* **69**, 3700–3710.
62. Borbas, K. E., H. L. Kee, D. Holten and J. S. Lindsey (2008) A compact water-soluble porphyrin bearing an iodoacetamido bioconjugatable site. *Org. Biomol. Chem.* **6**, 187–194.
63. Hambright, P. (2000) Chemistry of water soluble porphyrins. In *The Porphyrin Handbook*, Vol. 3 (Edited by K. M. Kadish, K. M. Smith and R. Guilard), pp. 129–210. Academic Press, San Diego.
64. Loudet, A. and K. Burgess (2007) BODIPY dyes and their derivatives: Syntheses and spectroscopic properties. *Chem. Rev.* **107**, 4891–4932.
65. Umezawa, K., Y. Nakamura, H. Makino, D. Citterio and K. Suzuki (2008) Bright, color-tunable fluorescent dyes in the visible–near-infrared region. *J. Am. Chem. Soc.* **130**, 1550–1551.